nature communications

Article

https://doi.org/10.1038/s41467-024-53311-4

Putting the squeeze on valence tautomerism in cobalt-dioxolene complexes

Received: 19 May 2024

Accepted: 9 October 2024

Published online: 16 October 2024

Check for updates

Aston Summers[1], F. Zahra M. Zahir[2], Gemma F. Turner[1], Moya A. Hay[2], Alan Riboldi-Tunnicliffe[3], Rachel Williamson[3], Stephanie Bird[3], Lars Goerigk[2] ✉, Colette Boskovic[2] ✉ & Stephen A. Moggach[1] ✉

Molecules that can reversibly switch between electronic states under an external stimulus are of interest to numerous applications. Complexes of open shell metal ions with redox active ligands undergo valence tautomerism, resulting in magnetic, colour and structural switching, relevant to data storage and actuators. However, the precise structural changes occurring during valence tautomerism in the solid state are unclear due to the lack of atomic-resolution characterization. Here, variable temperature and high-pressure single crystal X-ray diffraction is used to characterize valence tautomerism in two isostructural cobalt complexes, [Co(bis(6-methyl-2-pyridylmethyl) amine)(3,5-di-tert-butyl-1,2-dioxolene)]$^{+}$ and [Co(tris(6-methyl-2-pyridylmethyl) amine)(3,5-di-tert-butyl-1,2-dioxolene)]$^{+}$ to atomic resolution. The less sterically hindered dimethylated complex exhibits two-step thermally-induced interconversion between the high-spin Co^{II}-seminquinonate and low-spin Co^{III}-catecholate forms (valence tautomerism) at 155 and 95 K due to the presence of two symmetry-independent complexes. In contrast, the more sterically hindered trimethylated complex does not display thermal valence tautomerism. Both complexes exhibit unique behaviour under high pressure. The dimethylated species undergoes gradual, one-step valence tautomerism in both symmetry-independent complexes concurrently between 0.43 GPa and 1.30 GPa. In the trimethylated species, pressure is sufficient to overcome steric hindrance, leading to one-step valence tautomerism between 2.60 GPa and 3.10 GPa, demonstrating pressure-triggered valence tautomerism in a thermally inactive complex. This study is among the few investigations using in situ high-pressure single crystal X-ray diffraction to achieve atomic-level structural characterization of valence tautomerism, aiding the development of robust structure-property relationships in these types of complexes.

Molecules that can be reversibly switched between distinguishable forms by an external stimulus are of interest for numerous applications, including high density magnetic data storage and molecular actuators[1,2]. Complexes containing open shell metal ions offer elegant possibilities in this regard, based on the significant modifications of many physical properties that are accompanied by changes to the electronic structure of the metal ion. One example of molecular switching arises from the phenomenon of valence tautomerism, which

[1]School of Molecular Sciences, University of Western Australia, Crowley, Western Australia, Australia. [2]School of Chemistry, University of Melbourne, Parkville, VIC, Australia. [3]Australian Synchrotron, Clayton, VIC, Australia. ✉e-mail: lars.goerigk@unimelb.edu.au; c.boskovic@unimelb.edu.au; stephen.moggach@uwa.edu.au

involves stimulated intramolecular electron transfer between a metal and coordinated redox-active ligand[3,4]. Most examples of valence tautomerism arise from cobalt-dioxolene complexes that are interconverted between the diamagnetic low-spin Co^{III}-catecholato (LS-Co^{III}-Cat) and paramagnetic high-spin Co^{II}-semiquinonato (HS-Co^{II}-SQ) tautomers (Fig. 1a, b). Upon heating and cooling, a reversible thermal LS-Co^{III}-Cat to HS-Co^{II}-SQ intercoversion can be driven by the greater vibrational entropy of the HS-Co^{II}-SQ tautomer, associated with longer Co−O/N bond lengths and greater electronic entropy arising from the higher spin state degeneracy[5]. The two tautomers can be readily distinguished by colour, magnetic susceptibility and changes in the metal-donor atom and redox-active ligand bond lengths. While thermally- and photo-induced valence tautomerism has been explored extensively, less is known about pressure-induced valence tautomerism[6–9].

A family of complexes susceptible to valence tautomerism are $[Co(Me_ntpa)(dbdiox)]^+$ (Me_ntpa = *tris*(2-pyridylmethyl)amine where $n = 0 - 3$, corresponds to successive methylation of the 6-position of the pyridine rings, dbdiox = 3,5-di-*tert*-butyl-1,2-dioxolene)[5–7,9–14]. Previous analysis of valence tautomerism in this family of complexes by NMR and electronic spectroscopies, magnetic susceptibility and X-ray diffraction established that the charge distribution of the complex and its response to an external stimulus depends on the extent of methylation of the tpa ligand[5,7,10]. Magnetic susceptibility measurements indicated that both the dimethylated $[Co(Me_2tpa)(dbdiox)][PF_6]$.(toluene) (denoted hereafter as $[Me_2tpa]$) and trimethylated $[Co(Me_3tpa)(dbdiox)][PF_6]$.(toluene) (denoted hereafter as $[Me_3tpa]$) species were in the HS-Co^{II}-SQ form under ambient conditions in the solid state[5]. Incremental cooling of $[Me_2tpa]$ resulted in a gradual decrease in the magnetic susceptibility, corresponding to conversion to the LS-Co^{III}-Cat form below 280 K, with subtle two-step behaviour occurring at 155 K and 95 K. By contrast, $[Me_3tpa]$ remained in the HS-Co^{II}-SQ form over the whole temperature range between 320 K and 2 K, due to the increased steric bulk of the tpa ligand, which blocked the formation of the lower-volume, LS-Co^{III}-Cat tautomer[5]. In previous studies, crystal structures of $[Me_2tpa]$ and $[Me_3tpa]$ were only determined to 150 K, so any structural changes caused by valence tautomerism were not determined[5]. Photomagnetic measurements have revealed that $[Me_2tpa]$ also undergoes light-induced valence tautomerism[11]. For $[Me_2tpa]$, Caracciolo et al. (using magnetometry and NMR measurements) found that the application of pressure gradually increased the temperature of the HS-Co^{II}-SQ to LS-Co^{III}-Cat conversion until it reached room temperature at 1 GPa[7]. Pressure-induced valence tautomerism has not been probed at all for $[Me_3tpa]$. While thermal valence tautomerism is driven by entropy, pressure-induced processes are driven by volumetric changes in the complex or crystal, generating distinct electronic and structural responses. Here, temperature and pressure-induced valence tautomerism in $[Me_2tpa]$ and $[Me_3tpa]$ is assessed by single crystal X-ray diffraction at variable temperature and variable pressure, providing atomic resolution-structures to complement previously published magnetic and spectroscopic data for

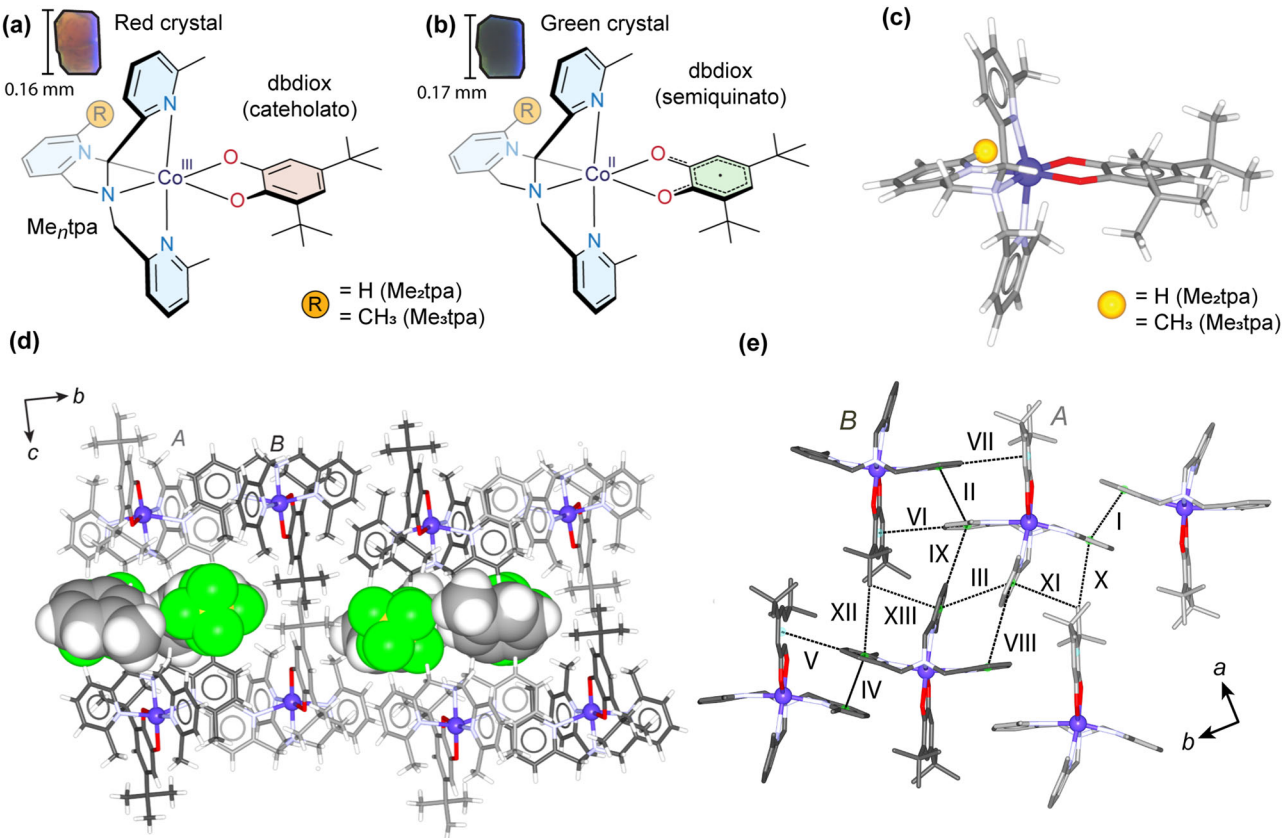

Fig. 1 | Chemical and crystal structure of valence tautomers. a Molecular diagram of $[Co(Me_ntpa)(dbdiox)]^+$ (where $n = 2$ (Me_2tpa) or 3 (Me_3tpa) (shaded blue)) as the LS-Co^{III}-Cat valence tautomer (shaded red), with a photograph of the red single crystal inset (**a**) or the HS-Co^{II}-SQ tautomer (shaded green), with a photograph of the green single crystal inset (**b**, **c**). Molecular structure of $[Co(Me_ntpa)(dbdiox)]^+$. The yellow sphere represents either a hydrogen atom in $[Co(Me_2tpa)(dbdiox)]^+$ or a methyl group in $[Co(Me_3tpa)(dbdiox)]^+$. In Me_2tpa the Me_2tpa ligand is disordered over two binding configurations in a 60:40 ratio (not shown). Atoms are coloured as follows: Co – dark blue, O – red, N – light blue, C – grey and H – white. **d** Packed structure of $[Co(Me_ntpa)(dbdiox)]^+$ viewed along the *a*-axis, showing alternating layers of complex molecules (stick model) and solvate (space-filled model). The lighter and darker coloured molecules distinguish the two symmetry-independent molecules, labelled A and B. **e** Intermolecular CH•••π and π•••π interactions (labelled I – XIII) within each layer of molecules in Me_2tpa and Me_3tpa. Molecules A and B are coloured with light and dark carbon atoms, respectively.

[Me_2tpa][5], in addition to pressure-induced valence tautomerism in [Me_3tpa].

Results and Discussion

Under ambient conditions, [Me_2tpa] and [Me_3tpa] form dark-green, isostructural crystals in the monoclinic space group, $P2_1/c$, with two symmetry-independent molecules in the asymmetric unit (labelled A and B in Figure S1). The cobalt centres adopt a distorted octahedral coordination. In [Me_2tpa], the dimethylated tpa ligand is disordered over two binding configurations with 60% and 40% crystallographic occupancy. Similar disorder in the binding configuration is reported for the monomethylated ligand, Metpa, in [Co(Metpa)(dbdiox)][PF_6].(toluene)[5]. One t-butyl group on one of the symmetry-independent molecules (A) is also rotationally disordered in both Me_2tpa and Me_3tpa under ambient conditions.

The charge distribution of the complexes can be determined by the lengths of Co–O/N coordination bonds, and C–O bonds in the redox-active dbdiox ligand. According to the previously reported structural and magnetic data for [Me_2tpa] and [Me_3tpa] at ambient pressure, 150 K and 160 K, the LS-Co^{III}-Cat tautomer has Co–O/N lengths of ~1.95 Å and C–O lengths of ~1.34 Å, while the HS-Co^{II}-SQ tautomer has Co–O/N lengths of ~2.14 Å and C–O lengths of ~1.29 Å[5,11]. Through fitting the bond lengths of an *o*-dioxolene ligand to a series of *o*-dioxolene species with known oxidation states, the metrical oxidation state (MOS) of the ligand can be calculated, with a value of −1 or −2 indicating the semiquinonato or catecholato tautomer, respectively[15]. From the crystal structures under ambient conditions, both [Me_2tpa] and [Me_3tpa] are in the HS-Co^{II}-SQ form, with MOS values close to −1 (Supplementary Tables S9/10), in agreement with previously reported magnetic data[5]. In [Me_2tpa], the symmetry-independent molecules, A and B, have average Co–O/N lengths of 2.1311(21) Å and 2.1263(21) Å and average C–O lengths of 1.286(7) Å and 1.277(7) Å. Similarly, A and B in [Me_3tpa] have average Co–O/N lengths of 2.1576(15) Å and 2.1551(16) Å, and average C–O lengths of 1.274(6) Å and 1.278(5) Å.

The supramolecular structures of [Me_2tpa] and [Me_3tpa] feature alternating layers of complexes and solvate that stack along the *c*-axis direction (Fig. 1d). Complexes within each layer interact through a variety of intermolecular interactions, including π•••π (I-IV), CH•••π (pyridyl•••dbdiox, V-VII, IX), CH•••π pyridyl•••pyridyl (VIII) and CH•••π interactions between the methyl•••pyridyl (X-XIII, Fig. 1e, Supplementary Figs. S12-19, Supplementary Tables S13-19).

To assess valence tautomerism in [Me_2tpa], its crystal structure was determined at 298 K, 155 K and 95 K under ambient pressure, and then between ambient pressure and 1.90 GPa in ~0.3 GPa steps at ambient temperature (298 K). The structure of [Me_3tpa] was determined at 298 K and 100 K, and then between ambient pressure and 4.40 GPa in ~0.5 GPa steps under ambient temperature (298 K). Crystallographic data are provided in Supplementary Tables S1–2, and structural data are displayed in Supplementary Tables S3–9 and Supplementary Figs. S2–23.

In agreement with previous reports[5], [Me_3tpa] does not undergo thermally-induced valence tautomerism, remaining in the HS-Co^{II}-SQ form between 298 K and 100 K. The less sterically bulky [Me_2tpa] complex, however, undergoes a two-step conversion from the HS-Co^{II}-SQ tautomer to the LS-Co^{III}-Cat tautomer upon cooling to 95 K due to the presence of the two symmetry-independent complexes, A and B. This is consistent with published magnetic susceptibility data[5]. Initial cooling from 298 K to 155 K stimulated the valence tautomeric interconversion between the HS-Co^{II}-SQ tautomer and the LS-Co^{III}-Cat tautomer in B (Fig. 1d). This interconversion was characterised by shortening of the average Co–O/N bonds by 7.2%, from 2.1263(21) Å at 298 K to 1.9773(19) Å at 155 K, and a lowering of the MOS to −2 in B (Fig. 2b, Supplementary Fig. S4, Supplementary Tables S5–6,10). These bond length changes are accompanied by a decrease in the angular distortion of the CoN_4O_2 octahedron, Σ, defined as the total deviation of the internal angles away from a perfect octahedron, from 96.1(8)° to 58.3(7)° (Supplementary Fig. S5), which is characteristic of formation of the LS-Co^{III}-Cat tautomer[16,17]. Meanwhile, a comparatively subtle shortening of Co–O/N by an average of 1.7% is observed for A, reducing to 2.0950(20) Å at 155 K. A minor decrease in the angular distortion of CoN_4O_2 also takes place on reducing temperature to 155 K, however, the MOS of A remained at −1.

Cooling from 155 K to 95 K prompts the valence tautomeric interconversion from the HS-Co^{II}-SQ tautomer to the LS-Co^{III}-Cat tautomer in A, evidenced by a pronounced shortening of the average Co–O/N length by 4.9% to 1.9952(21) Å and a decrease in the ligand MOS to −2, compared with subtle shortening of the average Co–O/N length by 0.5% in B. The angular distortion within CoN_4O_2, defined as the sum deviation of each internal angle within the octahedron away from 90°, in A decreases from 91.2(8)° to 67.9(8)° in this temperature range. Two-step spin transitions or valence tautomerism are often caused by steric effects at one or more crystallographically independent metal centres, which increase the energy barrier of the transition/interconversion[18,19]. In [Me_2tpa], A is closer to the surrounding PF_6^- counterions and toluene solvate than B. A noticeably short π•••π interaction is also formed between two A-molecules (interaction I in Fig. 1e). It is likely that these factors lead to valence tautomerism occurring in B at a higher temperature (155 K) than A (95 K). [Me_2tpa] also becomes more disordered upon cooling from 298 K to 155 K, then further to 95 K, with the t-butyl group in A becoming rotationally disordered at 155 K, followed by the same disorder occurring in B at 95 K. This order to disorder transition upon cooling coincides with A and B moving closer together in the asymmetric unit (by ~0.3 Å) between 298 and 95 K. The reasoning for this subtle crystallographic behaviour, however, is unclear, and whether it is linked to valence tautomerism needs further investigation.

Shortening of the Co–O/N bonds upon formation of the LS-Co^{III}-Cat state between 298 K and 95 K, in conjunction with thermal contraction of the crystal, causes the unit cell volume to decrease by a total of 5.8%, with shortening of the *a*, *b* and *c*-axes by 1.5%, 3.0% and 1.4%, respectively (Fig. 2a, Supplementary Table S3). The *a* and *c*-axes undergo the least amount of contraction as these axes are coincident with the orientation of the bulky t-butyl groups of the dbdiox ligand. As the unit cell volume contracts between 298 K and 95 K, all intermolecular interactions except interactions X, XII and XIII shorten by between 9.4% and 1.2% (average shortening of 2.5%), with interaction II (a π•••π interaction between pyridyl rings in A and B) shortening substantially (8.8%, Fig. 1e, Supplementary Figs. S13–15 and Supplementary Tables S10–11).

Pressure-induced valence tautomerism was assessed by compressing a single crystal of each [Me_2tpa] and [Me_3tpa] in a modified Merrill-Bassett diamond anvil cell, with low viscosity cryo oil (LVCO5 CryOil™) used as the hydrostatic medium. A maximum pressure of 4.50 GPa for Me_2tpa and 4.40 GPa Me_3tpa was reached, above which pressure the single-crystal quality degraded, and the samples became polycrystalline. For [Me_2tpa], atomic positions were obtained up to 1.90 GPa, above which only the unit cell dimensions could be determined. The same occurred in [Me_3tpa] above 3.60 GPa. Valence tautomerism was signalled by piezochromism with the crystals changing colour from green to red, and structural discontinuities in the complex and crystal during compression. Evolution of the crystal colouration and unit cell dimensions of [Me_2tpa] and [Me_3tpa] under applied hydrostatic pressure are shown in Fig. 2.

Gradual compression of [Me_2tpa] from ambient pressure to 1.90 GPa resulted in a colour change of the crystal from green to red, occurring primarily between 0.43 GPa and 1.30 GPa, indicative of the HS-Co^{II}-SQ to LS-Co^{III}-Cat conversion. The red colour was retained until 1.90 GPa and the green colour returned upon full pressure release. According to the Co–O/N coordination bond lengths in CoN_4O_2, valence tautomerism occurs gradually in a single step between

https://doi.org/10.1038/s41467-024-53311-4

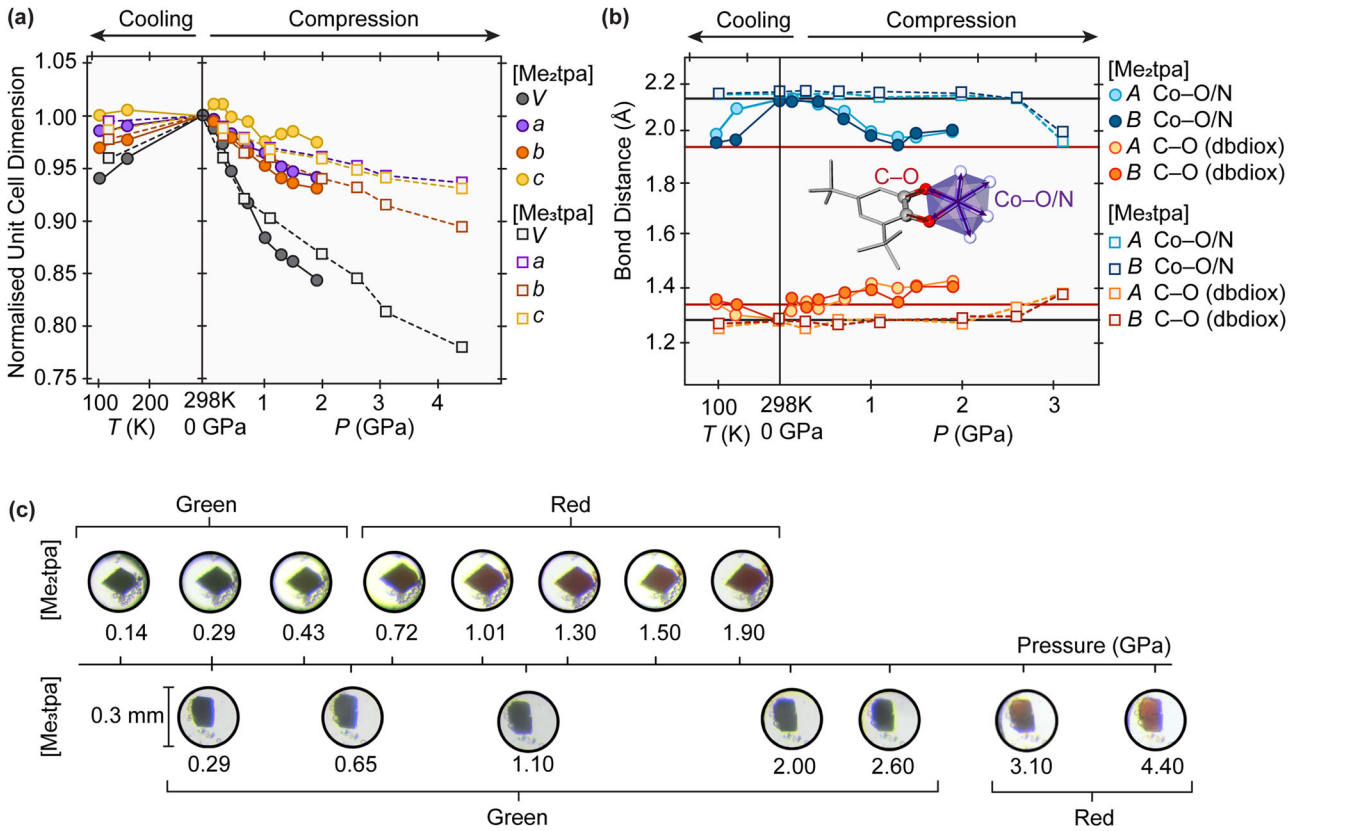

Fig. 2 | Structural and colour changes under temperature and pressure. a Plot of the relative change in unit cell dimensions of [Me_2tpa] (circles) and [Me_3tpa] (squares) at variable temperature and pressure. **b** Plot of the Co–O/N (shades of blue), and C–O bond lengths (shades of orange) in [Me_2tpa] (circles) and [Me_3tpa] (squares) for each symmetry-independent molecule, A (light shades) and B (dark shades). Black horizontal lines represent the expected values of the Co–O/N and C–O bond lengths for the HS-Co^{II}-SQ tautomer and the red horizontal lines represent the expected values for the LS-Co^{III}-Cat tautomer. **c** Photographs of [Me_2tpa] (upper) and [Me_3tpa] (lower) single crystals during compression in a modified Merrill-Bassett diamond anvil cell, showing a change in colour from green HS-Co^{II}-SQ to red LS-Co^{III}-Cat.

0.43 GPa and 1.30 GPa. In this pressure range the Co–O/N bond lengths in both symmetry-independent molecules shortened by ~7-8% to 1.991(11) Å for A and 1.960(11) Å for B. This is indicative of a gradual increase in the proportion of molecules in the LS-Co^{III}-Cat form. This is confirmed by the reduction in the angular distortion of the octahedral sphere in both complexes by 67% and 58% for A and B respectively between 0.43 GPa and 1.30 GPa (Supplementary Table S5), consistent with formation of the LS-Co^{III}-Cat state in both molecules. The Co–O/N bond lengths, octahedral distortion values and colour of the single-crystal sample remain relatively constant between 1.30 GPa and 1.90 GPa indicating the cessation of any valence tautomeric interconversion at 1.30 GPa.

In contrast, the MOS appears to change almost immediately on application of pressure to 0.14 GPa and increases to a minimum of approximately −2.5. This discrepancy is likely an artifact of the large error on C–C and C–O bond lengths as a result of the low-completeness of the data, which is not unusual for high-pressure single-crystal data. Unlike the thermal process, the pressure-induced valence tautomerism appears to occur simultaneously in both symmetry-independent molecules. However, we cannot rule out a two-step process at pressure, as smaller pressure increments may be necessary to observe this, which is near impossible in a diamond anvil cell.

The structural effect of valence tautomerism on the crystal of [Me_2tpa] can be followed by evolution of the unit cell dimensions during compression. Between ambient pressure and 1.90 GPa, the *a*, *b* and *c*-axes shorten by 5.829(6)%, 6.783(7) % and 3.91(5) %, respectively.

Pressure-induced valence tautomerism in [Me_3tpa] occurs at a much higher pressure than for [Me_2tpa], occurring in one step between 2.60 GPa and 3.10 GPa, signalled by a colour change of the crystal from green to red and changes in the Co–O/N (CoN_2O_4) and C–O bond (dbdiox) lengths corresponding to a decrease in the MOS of the ligand from −1 to −2 (Supplementary Table S10). The average Co–O/N lengths shortened to 1.972(9) Å and 2.008(9) and the average C–O bonds lengthened to 1.405(42) Å and 1.39(3) at 3.10 GPa for A and B respectively, characteristic of the LS-Co^{III}-Cat tautomer. The angular distortion, Σ, of both complexes dramatically decreases from ~100° to ~60° during valence tautomerism. These changes in molecular geometry are in line with those seen in [Me_2tpa] because of valence tautomerism, indicating that the conversion has progressed to completion. Despite the lack of data of atomic resolution obtained after 3.10 GPa, this cessation of valence tautomerism at 3.10 GPa is supported by the decrease in compressibility of the unit cell volume seen between 3.10 GPa and 4.40 GPa. The green colour is returned upon full pressure release. Notably, this complex does not exhibit thermally-induced valence tautomerism due to the additional steric bulk of the trimethylated tpa ligand. Therefore, high-pressure overcomes the steric barrier, enabling access to the lower-volume LS-Co^{III}-Cat tautomer.

To assess the structural mechanism by which pressure-induced valence tautomerism occurs in [Me_3tpa], we aimed to quantify the steric hindrance around the tpa ligand as a function of pressure. This was accomplished by measuring the distance between the methyl substituents on the tpa ligand as a triangular area (denoted tpa-Δ), defined with each vertex at the carbon bound to a methyl C-atom (Fig. 3a). When [Me_2tpa] and [Me_3tpa] are both in the HS-Co^{II}-SQ form at room temperature, the tpa-Δ measured 8.29(4) $Å^2$ and 8.10(5) $Å^2$ for A and B respectively in [Me_2tpa], compared to 8.546(23) $Å^2$ and

https://doi.org/10.1038/s41467-024-53311-4

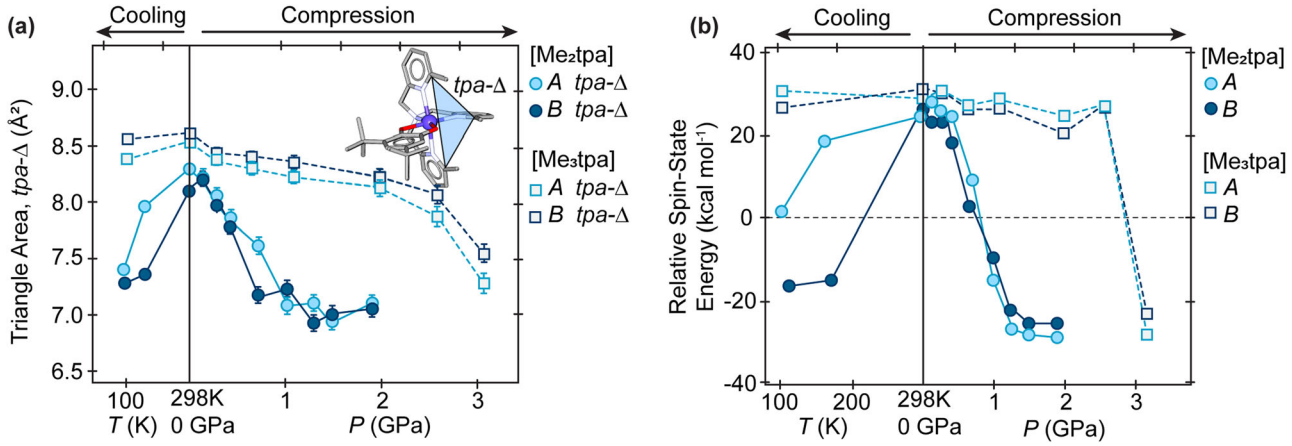

Fig. 3 | Ligand geometry and relative spin-state energy. a Plot of the tpa-Δ in [Me$_3$tpa] (squares, dashed lines) and [Me$_2$tpa] (circles, solid lines) at variable temperature and pressure. Values for both symmetry-independent complexes, A (light blue) and B (dark blue) is given. A diagram of the triangular area, the tpa-Δ, in the tpa complexes, with vertices on the methyl-bearing carbon atom, is overlaid. Vertical error bars are calculated from the estimated standard deviations on tpa-Δ from the crystal structures. **b** Plot of relative spin-state energy (ΔE) vs applied stimuli, for [Me$_2$tpa] (circles) and [Me$_3$tpa] (squares) for each symmetry-independent molecule, A (light blue) and B (dark blue).

8.620(24) Å^2 for A and B in [Me$_3$tpa] respectively. When [Me$_2$tpa] was in the LS-Co^{III}-Cat form at low temperature, the tpa-Δ was substantially smaller, measuring 7.42(4) Å^2 and 7.28(4) Å^2 for A and B respectively.

On undergoing valence tautomerism, the tpa-Δ dramatically decreased due to the reduction in the entire molecular volume, as indicated in Fig. 3a for [Me$_2$tpa] on cooling to 95 K or increasing pressure to ~1 GPa, with the tpa-Δ measuring ~7.3 Å^2 under both conditions. Upon application of pressure to [Me$_3$tpa], the Me$_3$tpa ligand compresses, causing the tpa-Δ to decrease by ~0.4 Å^2 until 2.6 GPa, at which the tpa-Δ for [Me$_3$tpa] reached approximately the same value as [Me$_2$tpa] under ambient conditions (~8.2 Å^2 for both molecules). Further compression of [Me$_3$tpa] to 3.10 GPa, resulted in contraction of the tpa-Δ in both independent molecules to ~7.3 Å^2. This demonstrates the capacity for pressure to facilitate valence tautomerism in [Me$_3$tpa] through compression of the tpa ligand, overcoming the increased steric bulk due to the additional methyl group.

Valence tautomerism and structural distortion is represented by anisotropic compression of the unit cell. Between ambient pressure and 3.10 GPa, the unit cell volume of [Me$_3$tpa] contracts by a total of 1565(6) Å^3 (−18.6%), with a significant increase in compressibility between 2.60 GPa and 3.10 GPa due to valence tautomerism. This compression corresponds to a bulk modulus, K_0, of 4(3) GPa from a third-order Birch-Murnaghan equation of state, calculated between ambient pressure and 2.60 GPa (as to exclude the new phase formed by valence tautomerism)[20]. This is particularly soft for a crystalline material, even for an organometallic complex, which in general have bulk moduli in the 7–10 GPa range[21–23]. Between ambient pressure and 3.10 GPa, the *a*, *b* and *c*-axes shorten by 6.409(13)%, 10.56(9)% and 6.765(13)% respectively, broadly similar to [Me$_2$tpa].

Contraction of the unit cell volume in [Me$_2$tpa] and [Me$_3$tpa] under pressure and during valence tautomerism derives from compression of both the molecular and supramolecular structures. Compression of the supramolecular structure is facilitated by shortening of intermolecular π•••π and CH•••π distances by between 6.7% to 15.4% (average = −9.7%) and 6.8% to 7.6% (average = −7.3%), respectively, between ambient pressure and 1.90 GPa in [Me$_2$tpa], and between 8.6% to 17.9% (π•••π, average = −12.5%), and 8.8% to 12.8% (CH•••π, average = −10.4%) between ambient pressure and 3.10 GPa in [Me$_3$tpa]. Upon valence tautomerism in both [Me$_2$tpa] and [Me$_3$tpa] many of these interactions show substantial changes in their compressibility. This is most apparent in the π•••π interactions; two of the interactions, II and IV, show a substantial increase in compressibility, whereas there is a negligible increase in compressibility for interactions I and III. Specifically, in [Me$_2$tpa], 44% of the compression of interaction I occurs during valence tautomerism (0.43 GPa–1.30 GPa) compared to 78% for interaction II. This is substantially more pronounced in [Me$_3$tpa] where only 7.7% of the compression of interaction I occurs during valence tautomerism (2.6 GPa–3.10 GPa) compared to 64% for interaction II. Similar behaviour is seen across the CH•••π interactions with the majority becoming more compressible upon valence tautomerism. However, unlike any of the π•••π interactions, interactions V, X and XIII expand substantially during valence tautomerism in both [Me$_2$tpa] and [Me$_3$tpa]. The vast differences in behaviour of these interactions upon valence tautomerism highlights the strong relationship between the molecular rearrangement caused by valence tautomerism and the supramolecular structure. To fully understand whether the changes in these interactions aid or hinder the stabilisation of the LS-Co^{III}-Cat tautomer and the cooperativity of the conversion, a hierarchy of energies for each of the intermolecular interactions for each pressure would be needed; a notable point of future work.

The influence of structural variation on the spin-state energetics of the tautomers was assessed via density functional theory (DFT) calculations. The previously identified[24,25] M06L-D4/ZORA-def2-TZVPP[26–30] method generally offers reliable spin-state energies for cobalt-dioxolene complexes. The relative spin-state energy of the tautomers ($\Delta E = E$ LS-Co^{III}-Cat − E HS-Co^{II}-SQ) were determined on each crystallographically independent molecule (A and B) of [Me$_2$tpa] and [Me$_3$tpa] at respective pressure/temperature points, using the constrained geometries from the crystal structures without further optimisation to encapsulate structural features (Fig. 3b, Supplementary Tables S11–S12). Employing special force-field methods[31,32] to simulate pressure effects on quantum-chemically obtained geometries led to unreasonably distorted structures, or required excessively high pressure, indicating the ongoing need for further development in this area.

The calculated ΔE with varying pressure highlights that compression assists in surpassing the spin-state energy requirements. As illustrated in Fig. 3b, at ambient conditions, the ground state of [Me$_2$tpa] and [Me$_3$tpa] is the HS-Co^{II}-SQ form ($\Delta E > 0$). Elevating pressure results in a progressive reduction of ΔE to reach equilibrium ($\Delta E = 0$), denoting the critical pressure. Further increases in pressure caused ΔE to be negative, favouring the formation of the LS-Co^{III}-Cat tautomer. The correlation of relative spin-state energy at varying pressure for both A and B for [Me$_2$tpa] and [Me$_3$tpa] aligns effectively

with the tpa-Δ as well as Co-O/N bond distances. The energy requirement for interconversion of [Me_3tpa] is not met until 3.10 GPa. Increasing the pressure causes both A and B to undergo concurrent switching between 2.60 GPa and 3.10 GPa ($\Delta E = +27$ kcal mol^{-1} at 2.60 GPa for A and B, to $\Delta E = -31.1$ kcal mol^{-1} for A and $\Delta E = -26.3$ kcal mol^{-1} for B at 3.10 GPa). Similar to [Me_3tpa], A and B of [Me_2tpa] display a simultaneous transition, but at relatively smaller applied pressure between 0.43 GPa and 1.3 GPa with a critical pressure of 0.7 GPa ($\Delta E = 0$), as a unified single-step process. In contrast, upon thermal stimulation, [Me_2tpa] exhibits a well resolved two-step process wherein the transition of B precedes that of A. The calculated switching points and transition features for both [Me_2tpa] and [Me_3tpa] align remarkably well with both pressure-induced and thermally-induced valence tautomeric traits seen in experimental measurements.

Here we report pressure-induced valence tautomerism in two cobalt-dioxolene complexes, [Me_2tpa] and [Me_3tpa], using a combination of single-crystal X-ray diffraction, high-pressure diamond anvil cell techniques, and density functional theory calculations. [Me_2tpa] undergoes a two-step transition from the HS-Co^{II}-SQ form to the LS-Co^{III}-Cat form upon cooling due to the presence of two symmetry-independent molecules. In contrast, [Me_3tpa] does not exhibit thermally induced valence tautomerism due to increased steric bulk. Applying pressure facilitates valence tautomerism in both complexes. [Me_2tpa] undergoes a single-step transition at a lower pressure (0.43 GPa–1.30 GPa) compared to [Me_3tpa] (2.60 GPa–3.10 GPa) due to its less sterically hindered tpa ligand.

Valence tautomerism leads to a decrease in unit cell volume and changes in intermolecular interactions. These changes highlight the interplay between the molecular rearrangement and the surrounding supramolecular structure, while DFT calculations support the experimental observations, demonstrating that pressure progressively reduces the energy barrier for the transition to the LS-Co^{III}-Cat form. Such insights are necessary to understand structure-property relationships in VT complexes, highlighting the importance of using both variable temperature and high-pressure single crystal X-ray diffraction to elucidate atomic-resolution structural changes during VT.

Following this pressure study, it is notable that valence tautomerism in [Me_2tpa] can be induced by thermal, light and pressure stimuli, paving the way for applications that require multi-stimuli responses. In the future, we aim to investigate the individual energies of intermolecular interactions to understand their role in stabilising the LS-Co^{III}-Cat tautomer. We also aim to further develop methods to accurately simulate pressure effects on quantum-chemically obtained geometries. Overall, this study provides valuable insights into the interplay between pressure, temperature, and steric effects in controlling valence tautomerism in cobalt-dioxolene complexes. This knowledge could be crucial for designing future functional materials with desired properties.

Methods

Synthesis of ligands and complexes

Synthesis of the complexes was performed using standard Schlenk line techniques under a nitrogen atmosphere. All chemicals used were of reagent grade and used as received. Methanol was dried using 3 Å sieves for three days and degassed through a minimum of ten cycles of vigorous shaking under vacuum and subsequent backfilling with nitrogen. The 3 Å sieves were activated by heating at 300 °C for 48 h and cooling under vacuum.

Bis((6-methyl-2-pyridyl)methyl)(2-pyridylmethyl)amine (ligand Me_2tpa)

This ligand was synthesized according to modified literature procedure[33]. Distilled 2-aminomethylpyridine (0.89 g, 8.3 mmol) and 6-methyl-2-pyridine carboxaldehyde (2.00 g, 16.5 mmol) were added to a stirred dichloromethane (200 mL) solution of sodium triacetoxyborohydride (5.24 g, 24.7 mmol). The reaction mixture was covered with foil and left to stir for 48 h. A saturated aqueous solution of sodium hydrogencarbonate (2.08 g, 24.7 mmol) was added and the resulting solution was stirred for another 30 min. The organic phase was extracted with dichloromethane (20 mL × 3) and dried over $MgSO_4$ to give a dark yellow oil. The oil residue was extracted several times with hexane and removal of solvent afforded colourless needles of bis((6-methyl-2-pyridyl)methyl)(2-pyridylmethyl)amine in 90–95% yield.

Tris(6-methyl-2-pyridylmethyl)amine (ligand Me_3tpa)

The precursor 6-formaldoxime-2-methylpyridine was synthesized from 6-methyl-2-pyridine carboxaldehyde based on reported procedures[34]. The resulting solid was subsequently dried in the presence of phosphorous pentoxide. The ligand precursor 6-methyl-2-aminomethylpyridine was synthesized using a modified literature procedure[34]. Product yield was maximized by preparing a dry and degassed methanolic solution of 6-formaldoxime-2-methylpyridine (4 g/500 mL) with 10 wt% Pd/C. The reaction mixture was contained in a 3-neck enclosed round bottom flask and stirred under constant flow of hydrogen for up to 6–8 h. Using the modified literature procedure described above for ligand Me_2tpa[10], the yellow oil (6-methyl-2-aminomethylpyridine) was subjected to a reductive amination with 6-methyl-2-pyridine carboxaldehyde and sodium triacetoxyborohydride. The reaction afforded 95–98% yield of tris(6-methyl-2-pyridylmethyl)amine.

[Co(Me_2tpa)(dbdiox)][PF_6].(toluene), [Me_2tpa]

The synthesized organic ligand Me_2tpa (64 mg, 0.20 mmol) was added to a dried and degassed methanol solution (10 ml) of $CoCl_2.6H_2O$ (48 mg, 0.20 mmol). The resulting green solution was left stirring for 10 min under a nitrogen atmosphere. A dried and degassed methanol solution (10 ml) containing 3,5-di-*tert*-butylcatechol (37 mg, 0.20 mmol) was deprotonated with triethylamine (55 µL, 0.40 mmol) by stirring for 10 min. The deprotonated 3,5-di-*tert*-butylcatechol solution was slowly added to the cobalt-Me_2tpa mixture and stirred for 10 min to obtain a reddish-brown solution. The resulting solution was subjected to aerial oxidation followed by the addition of an aqueous KPF_6 solution to afford a black-green precipitate of [Co(Me_2tpa)(dbdiox)][PF_6]. The crude product was washed with diethyl ether (2 × 2 mL) and collected by vacuum filtration under ambient conditions. Large dark-green crystals were obtained by heating a moderately concentrated solution of toluene in a sand bath with subsequent slow cooling, affording [Co(Me_2tpa)(dbdiox)][PF_6].(toluene). Excess concentration resulted in co-crystallization of byproducts.

[Co(Me_3tpa)(dbdiox)][PF_6].(toluene), [Me_3tpa]

The synthesised organic ligand Me_3tpa (67 mg, 0.20 mmol) was added to a dried and degassed methanol solution (10 ml) of $CoCl_2.6H_2O$ (48 mg, 0.20 mmol). The resulting purple solution was left stirring for 10 minutes under a nitrogen atmosphere. A dried and degassed methanol solution (10 ml) containing 3,5-di-*tert*-butylcatechol (37 mg, 0.20 mmol) was deprotonated with triethylamine (55 µL, 0.40 mmol) by stirring for 10 min. The deprotonated 3,5-di-*tert*-butylcatechol solution was slowly added to the cobalt-Me_2tpa mixture and stirred for 10 min to obtain a reddish-brown solution. The resulting solution was subjected to aerial oxidation followed by the addition of an aqueous KPF_6 solution to obtain a black-green precipitate of [Co(Me_3tpa)(dbdiox)][PF_6]. The crude product was washed with diethyl ether (2 × 2 mL) and collected by vacuum filtration under ambient conditions. Large dark-green crystals were obtained by heating a moderately concentrated toluene solution in a sand bath with subsequent slow cooling affording Co(Me_3tpa)(dbdiox)][PF_6].(toluene).

Single crystal X-ray diffraction

Ambient conditions. Dull-green, block-shaped single crystals of each [Me_2tpa] and [Me_3tpa] were characterized by single crystal X-ray diffraction using a Rigaku Oxford Diffraction XtaLAB Synergy S diffractometer with MoKα radiation at $T = 293(2)$ K. Diffraction data were integrated and reduced in CrysAlisPro 1.171.40.84a[35]. Absorption effects were corrected using an empirical multi-scan correction using spherical harmonics in the same program. The structures were solved in $P2_1/c$ (# 14) by the ShelXT[36] structure solution program using iterative methods and refined by full matrix least squares minimisation on F^2 using ShelXL[37] in Olex2[38]. Hydrogen atoms were placed geometrically and constrained to ride on their host atoms.

Under ambient conditions, one of the t-butyl groups in [Me_3tpa] was disordered, and so was refined with 1,2 and 1,3 similarity restraints to ensure the group remained tetrahedral. The methyl C-atom anisotropic displacement parameters were constrained to be identical. In both [Me_2tpa] and [Me_3tpa], two toluene molecules were in the asymmetric unit, which were modelled as rigid bodies from the fragment database in Olex2[38]. The toluene C-atoms were refined using only isotropic thermal parameters because the data were collected at room temperature (to compare to the high-pressure data). The $[PF_6]^-$ counterions were also modelled as rigid fragments and with thermal similarity restraints.

Low Temperature

Dull-green, block-shaped single crystals of each [Me_2tpa] and [Me_3tpa] were characterized by single crystal X-ray diffraction using a Rigaku Oxford Diffraction XtaLAB Synergy S diffractometer with CuKα radiation at variable temperature. Structures of [Me_2tpa] were collected at 155 K and 95 K, while [Me_3tpa] was collected at 100 K. Diffraction data were integrated and reduced in CrysAlisPro 1.171.40.84a[35]. Absorption effects were corrected using an empirical multi-scan correction using spherical harmonics in the same program.

The maximum resolution that was achieved was $\theta = 75.592°$ (0.80 Å). The structures were solved in $P2_1/c$ (# 14) by the ShelXT[36] structure solution program using iterative methods and refined by full matrix least squares minimisation on F^2 using ShelXL[37] in Olex2[38]. Hydrogen atoms were placed geometrically and constrained to ride on their host atoms. Toluene solvate and $[PF_6]^-$ counterions were modelled as rigid fragments.

High-Pressure, [Co(Me_3tpa)(dbdiox)][PF_6].(toluene)

A single-crystal of [Me_2tpa] and [Me_3tpa] was each loaded into a Merrill Bassett diamond anvil cell containing two Boehlar-Almax diamond anvils with 600 μm culet faces fixed to tungsten-carbide backing discs. The DAC had a 40° half-opening angle. A 300 μm hole was drilled through a 200 μm thick tungsten gasket and fixed to one of the diamond culets to create a cylindrical sample chamber. Ruby crystals were also loaded into the sample chamber and used as a pressure calibrant, measured using the ruby fluorescence technique[39,40].

The [Me_2tpa] crystal was then gradually compressed using MiTeGen LVCO-5 oil as a pressure transmitting medium from 0.14 to 1.90 GPa in ~0.5 GPa increments. The [Me_3tpa] crystal was gradually compressed in MiTeGen LVCO-5 oil from 0.29 to 4.40 GPa in ~0.5 GPa increments. Diffraction data were collected at each pressure increment for both samples on a Rigaku Oxford Diffraction XtaLAB Synergy S diffractometer at ambient temperature using Mo Kα radiation. Diffraction data were integrated and reduced in CrysAlisPro 1.171.40.84a[35], using a mask based on the 40° half-opening angle of the pressure cell to remove the shaded regions of the diffraction frames. Absorption effects were corrected using an empirical multi-scan correction using spherical harmonics in the same program.

The structure at each pressure was refined from the starting coordinates of the ambient pressure data. The structures were refined in an almost identical fashion to the ambient pressure data, except all t-butyl groups pyridylmethyl-amine groups were refined as rigid bodies constructed from the low-temperature coordinates. Only the dioxolene fragment was allowed to refine freely. Only Co, P and F-atoms were refined with anisotropic displacement parameters, all other non-H atoms were refined with isotropic thermal parameters. Thermal similarity restraints were applied for all non-H atoms. This parameterisation strategy was used to reduce the number of refined parameters due to the low completeness of the high-pressure data, and the large number of independent atoms ($Z' = 2$, with solvent and counterions).

On increasing pressure to 3.1 GPa in [Me_3tpa], a solvent mask was used to model the two toluene solvent molecules. The solvent calculated equated to 340 electrons in a volume of 1048 Å^3 located in 1 void per unit cell. This was consistent with the presence of one toluene molecule per asymmetric unit (which accounts for 400 electrons per unit cell). The one disordered t-butyl group also became ordered at 3.1 GPa. All other refinement parametrisation was kept the same.

Computational methods

Density functional calculations were performed using the ORCA 4.0-4.1[41,42] quantum chemistry package. Atomic coordinates for single complexes were obtained from the crystal structures of [Me_2tpa] and [Me_3tpa] without further optimisation. Two crystallographically unique molecules A and B of complexes [Me_2tpa] and [Me_3tpa] were isolated from each other at each compression or cooling point. Single point calculations were independently performed on each complex using the density functional M06L[30] with DFT-D4[27] dispersion correction to account for London dispersion interactions considering atomic charge and spin states. Scalar relativistic effects were considered with the zeroth order regular approximation (ZORA)[29] model using the relativistically contracted ZORA-def2-TZVPP[29] atomic orbital basis set along with the segmented all electron relativistically contracted SARC/J auxiliary basis set[26]. The largest numerical quadrature grid (grid 7) was used in the calculations. The spin-unrestricted formalism was employed for the open shell high spin Co^{II}-semiquinonato tautomer. Calculations were conducted using the singlet state to represent the low spin Co^{III}-catecholato tautomer, and quintet state to represent high spin Co^{II}-semiquinonato tautomer of each molecule. The relative spin state energies were [$\Delta E = E$(low spin Co^{III}-catecholato) - E(high spin Co^{II}-semiquinonato)] obtained at each pressure or temperature point and plotted against the applied pressure or temperature.

Data availability

Crystallographic Information Files are available from the Cambridge Crystallographic Data Centre repository under accession codes: 2353216-2353234. Copies of the data can be obtained free of charge by visiting https://www.ccdc.cam.ac.uk/structures/, or Cambridge Crystallographic Data Centre, 12 Union Road, Cambridge CB2 1EZ, U.KCB21EZ, UK (fax +441223336033; deposit@ccdc.cam.ac.uk). Crystallographic, structural data and computational data are provided in the Supplementary Information file. All additional data are available from the corresponding author upon request.

References

1. Meng, Y.-S., Sato, O. & Liu, T. Manipulating metal-to-metal charge transfer for materials with switchable functionality. *Angew. Chem. Int. Ed.* **57**, 12216–12226 (2018).
2. Manrique-Juárez, M. D. et al. Switchable molecule-based materials for micro- and nanoscale actuating applications: achievements and prospects. *Coord. Chem. Rev.* **308**, 395–408 (2016).
3. Pierpont, C. G. Studies on charge distribution and valence tautomerism in transition metal complexes of catecholate and semiquinonate ligands. *Coord. Chem. Rev.* **216-217**, 99–125 (2001).
4. Tezgerevska, T., Alley, K. G. & Boskovic, C. Valence tautomerism in metal complexes: stimulated and reversible intramolecular

electron transfer between metal centers and organic ligands. *Coord. Chem. Rev.* **268**, 23–40 (2014).
5. Beni, A., Dei, A., Laschi, S., Rizzitano, M. & Sorace, L. Tuning the charge distribution and photoswitchable properties of cobalt–dioxolene complexes by using molecular techniques. *Chem. Eur. J.* **14**, 1804–1813 (2008).
6. Caneschi, A. et al. Pressure- and temperature-induced valence tautomeric interconversion in a o-Dioxolene adduct of a cobalt–tetraazamacrocycle complex. *Chem. Eur. J.* **7**, 3926–3930 (2001).
7. Caracciolo, F. et al. Spin fluctuations in the light-induced high-spin state of cobalt valence tautomers. *PRB* **98**, 054416 (2018).
8. Li, B. et al. The effects of pressure on valence tautomeric transitions of dinuclear cobalt complexes. *Chem. Commun*, 6019–6021 (2008).
9. Roux, C. et al. Pressure-induced valence tautomerism in cobalt o-Quinone complexes: an X-ray absorption study of the low-spin [CoIII(3,5-DTBSQ)(3,5-DTBCat)(phen)] to High-Spin [CoII(3,5-DTBSQ)2(phen)] Interconversion. *Inorg. Chem.* **35**, 2846–2852 (1996).
10. Beni, A., Dei, A., Rizzitano, M. & Sorace, L. Unprecedented optically induced long-lived intramolecular electron transfer in cobalt–dioxolene complexes. *Chem. Commun*, 2160–2162 https://doi.org/10.1039/B702932B (2007).
11. Dapporto, P., Dei, A., Poneti, G. & Sorace, L. Complete direct and reverse optically induced valence tautomeric interconversion in a cobalt–dioxolene complex. *Chem. Eur. J.* **14**, 10915–10918 (2008).
12. Gransbury, G. K. et al. Single-ion anisotropy and exchange coupling in cobalt(II)-radical complexes: insights from magnetic and ab initio studies. *Chem. Sci.* **10**, 8855–8871 (2019).
13. Gransbury, G. K. et al. DFT prediction and experimental investigation of valence tautomerism in cobalt-dioxolene complexes. *Inorg. Chem.* **58**, 4230–4243 (2019).
14. Starikova, A. A., Chegerev, M. G., Starikov, A. G. & Minkin, V. I. A DFT computational study of the magnetic behaviour of cobalt dioxolene complexes of tetraazamacrocyclic ligands. *Comput. Theor. Chem.* **1124**, 15–22 (2018).
15. Brown, S. N. Metrical oxidation states of 2-amidophenoxide and catecholate ligands: structural signatures of metal–ligand π bonding in potentially noninnocent ligands. *Inorg. Chem.* **51**, 1251–1260 (2012).
16. Gütlich, P., Gaspar, A. B. & Garcia, Y. Spin state switching in iron coordination compounds. *Beilstein J. Org. Chem.* **9**, 342–391 (2013).
17. Ketkaew, R. et al. OctaDist: a tool for calculating distortion parameters in spin crossover and coordination complexes. *Dalton Trans.* **50**, 1086–1096 (2021).
18. Ahmed, M. et al. Regulation of multistep spin crossover across multiple stimuli in a 2-D framework material. *Inorg. Chem.* **61**, 6641–6649 (2022).
19. Molnár, G. et al. Two-step spin-crossover phenomenon under high pressure in the coordination colymer Fe(3-methylpyridine)2[Ni(CN)4]. *Chem. Phys. Lett.* **423**, 152–156 (2006).
20. Gonzalez-Platas, J., Alvaro, M., Nestola, F. & Angel, R. EosFit7-GUI: a new graphical user interface for equation of state calculations, analyses and teaching. *J. Appl. Crystallogr.* **49**, 1377–1382 (2016).
21. Hazen, R. M., Hoering, T. C. & Hofmeister, A. M. Compressibility and high-pressure phase transition of a metalloporphyrin: (5,10,15,20-tetraphenyl-12H,23H-porphinato)cobalt(II). *J. Phys. Chem.* **91**, 5042–5045 (1987).
22. Shepherd, H. J. et al. Antagonism between extreme negative linear compression and spin crossover in $[Fe(dpp)_2(NCS)_2]$·py. *Angew. Chem. Int. Ed.* **51**, 3910–3914 (2012).
23. Slebodnick, C. et al. High pressure study of $Ru_3(CO)_{12}$ by X-ray diffraction, Raman, and infrared spectroscopy. *Inorg. Chem.* **43**, 5245–5252 (2004).
24. Zahir, F.Z.M. et al. Predicting valence tautomerism in diverse cobalt–dioxolene complexes: elucidation of the role of ligands and solvent. *Chem.Sci.* **15**, 5694–5710 (2024).
25. Janetzki, J. T. et al. A convenient DFT-based strategy for predicting transition temperatures of valence tautomeric molecular switches. *Inorg. Chem.* **60**, 14475–14487 (2021).
26. Pantazis, D. A., Chen, X.-Y., Landus, C. R. & Neese, F. All-electron scalar relativistic basis sets for third-row transition metal atoms. *J. Chem. Theory Comput.* **4**, 908–919 (2008).
27. Caldeweyher, E. et al. A generally applicable atomic-charge dependent London dispersion correction. *J. Chem. Phys.* **150** https://doi.org/10.1063/1.5090222 (2019).
28. van Lenthe, E., van Leeuwen, R., Baerends, E. J. & Snijders, J. G. Relativistic regular two-component hamiltonians. *Int. J. Quantum Chem.* **57**, 281–293 (1996).
29. Weigend, F. & Ahlrichs, R. Balanced basis sets of split valence, triple zeta valence and quadruple zeta valence quality for H to Rn: Design and Assessment of Accuracy. *Phys. Chem. Chem. Phys.* **7**, 3297–3305 (2005).
30. Zhao, Y. & Truhlar, D. G. A New Local Density Functional for Nain-Group Thermochemistry, Transition Metal Bonding, Thermochemical kinetics, and Noncovalent Interactions. *J. Chem. Phys.* **125** https://doi.org/10.1063/1.2370993 (2006).
31. Stauch, T. A mechanochemical model for the simulation of molecules and molecular crystals under hydrostatic pressure. *J. Chem. Phys.* **153** https://doi.org/10.1063/5.0024671 (2020).
32. Stauch, T., Chakraborty, R. & Head-Gordon, M. Quantum chemical modeling of pressure-induced spin crossover in octahedral metal-ligand complexes. *Chem. Phys. Chem.* **20**, 2742–2747 (2019).
33. Beni, A. et al. Tuning the charge distribution and photoswitchable properties of cobalt-dioxolene complexes by using molecular techniques. *Chem. Eur. J.* **14**, 1804–1813 (2008).
34. Fuentes, O. & Paulder, W. W. Synthesis of 2-Azacycl[3.2.2]Azine. *J. Org. Chem.* **40**, 1210–1213 (1975).
35. CrysAlisPro Software system v. 1.171.40.84a, Rigaku Corporation, Wroclaw, Poland (2020)
36. Sheldrick, G. M. SHELXT– integrated space-group and crystal-structure determination. *Acta Crystallogr.* **A71**, 3–8 (2015).
37. Sheldrick, G. M. Crystal structure refinement with SHELXL. *Acta Crystallogr.* **C71**, 3–8 (2015).
38. Dolomanov, O. V. et al. OLEX2: a complete structure solution, refinement and analysis program. *J. Appl. Crystallogr.* **42**, 339–341 (2009).
39. Mao, H. K., Bell, P. M., Shaner, J. W. & Steinberg, D. J. Specific volume measurements of Cu, Mo, Pd, and Ag and calibration of the ruby R1 fluorescence pressure gauge from 0.06 to 1 Mbar. *J. Appl. Phys.* **49**, 3276–3283 (1978).
40. Mao, H. K., Xu, J. & Bell, P. M. Calibration of the ruby pressure gauge to 800 kbar under quasi-hydrostatic conditions. *J. Geophys. Res.* **91**, 4673–4676 (1986).
41. Neese, F. The ORCA program system. *Wires Comput. Mol. Sci.* **2**, 73–78 (2012).
42. Neese, F. Software Update: the ORCA Program System, version 4.0. *Wires Comput. Mol. Sci.* **8**, https://doi.org/10.1002/wcms.1327 (2018).

Acknowledgements

A.S. acknowledges the Australian Government and the University of Western Australia for the provision of a Research Training Program Scholarship. F.Z.M.Z. acknowledges the Melbourne Research Scholarship. L.G. is grateful for generous allocations of computational resources from the National Computational Infrastructure (NCI) Facility within the National Computational Merit Allocation Scheme (project fk5), and Research Platform Services (ResPlat) at The University of Melbourne (project punim0094). S.A.M. acknowledges the Australian Research Council (ARC) for the provision of a Future Fellowship (FT200100243)

and a Discovery Project (DP220103690). G.F.T. is funded by DP220103690. C.B. acknowledges the ARC for funding a Discovery Project (DP19010085).

Author contributions

S.A.M., C.B., L.G., A.S., and F.Z.M.Z. conceived the experiments, A.S., F.Z.M.Z., and M.A.H. led data acquisition, A.R.T, R.W. and S.B. assisted with beamtime in MX1, A.S., G.F.T., and S.A.M. refined the crystal structures, A.S. and G.F.T. wrote the initial manuscript, and all authors offered further analysis and edited the manuscript.

Competing interests

The authors declare no competing interests.

Additional information

Supplementary information The online version contains supplementary material available at https://doi.org/10.1038/s41467-024-53311-4.

Correspondence and requests for materials should be addressed to Lars Goerigk, Colette Boskovic or Stephen A. Moggach.

Peer review information *Nature Communications* thanks Jun Tao and the other, anonymous, reviewer(s) for their contribution to the peer review of this work. A peer review file is available.